Forest Ecology and Management 545 (2023) 121299

Contents lists available at ScienceDirect

Forest Ecology and Management

journal homepage: www.elsevier.com/locate/foreco

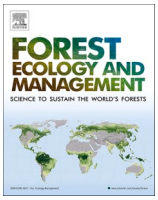

Carbon sequestration potential of eight economically important tree species in Northeast China under climate change

Lars Sprengel [a,b,*], Andreas Hamann [c], Shuirong Wu [d], Heinrich Spiecker [b]

[a] Department of Silviculture and Forest Ecology of the Temperate Zones, Georg-August-University Göttingen, Büsgenweg 1, 37077 Göttingen, Germany
[b] Chair of Forest Growth and Dendroecology, Albert-Ludwigs-University Freiburg, Tennenbacherstraße 4, 79106 Freiburg, Germany
[c] Department of Renewable Resources, University of Alberta, Edmonton, 733 General Services Building, Edmonton, AB T6G 2H1, Canada
[d] Research Institute of Forestry Policy and Information, Chinese Academy of Forestry, No. 1 Dongxiaofu, Haidian District, Beijing 100091, China

ARTICLE INFO

Keywords:
Forestry
Biomass
Heat moisture index
Response function analysis
Tree ring
Wood density

ABSTRACT

The carbon sequestration potential of forest ecosystems is expected to play a crucial role in mitigating global warming, depending on how climate change will affect tree growth under various local environmental conditions. Here, we investigated the climatic limiting factors for forest tree growth and future carbon sequestration potential for eight economically important forest tree species in Zhongtiao Mountains of Shanxi Province in China. Specifically, we test if moisture limitations compromise annual radial increments (ARI) and a carbon sequestration index (I_C), based on tree-rings and wood density. A bootstrapped response function analysis of historical detrended ARIs, reveals statistically significant moisture limitations in two or more summer months for half of the species investigated. Using a custom heat:moisture index based on these seasonal growth limitations, we predict I_C under multi-model CMIP6 climate change projections for the region. Under moderate future climate scenarios for the period 2041–2070, the carbon sequestration potential for most species is likely to increase significantly. This is because under current climate only some species experience moisture limitations, and a projected increase in seasonal precipitation mitigates these growth limitations. We conclude that model projections are favorable for carbon sequestration and future commercial forestry potential in the Zhongtiao Mountain forestry region.

1. Introduction

The Sixth Assessment Report of the Intergovernmental Panel on Climate Change indicates that global temperatures will almost certainly exceed 1.5 °C during the 21st century, and possibly breach the 2 °C limit, which is widely viewed as tipping point, where irreversible ecological impacts are expected (IPCC, 2021). Forest ecosystems belong to the largest terrestrial carbon sinks on the planet that can sequester large amounts of carbon annually and therefore contribute to climate change mitigation by removing CO_2 from the atmosphere (Bonan, 2008; Pan et al., 2011). However, the response of future forest growth to climate change is uncertain: increasing CO_2 could increase leaf-scale photosynthesis (Walker et al., 2021) and a warmer climate could prolong the vegetation period, but positive growth responses to climate warming may be transitory (D'Orangeville et al., 2018) or could be negative if limited by water availability (Babst et al., 2019). Specifically, increasing temperature may increase evapotranspirative demand, possibly exacerbated by trends of decreasing precipitation, and leading to drought stress reducing tree growth (Williams et al., 2020). A common response of trees to a drought year is a reduced annual radial increment during the year in which the drought occurred (Chen et al., 2010; Hipler et al., 2020; Larysch et al., 2022), and depending on the drought severity also in the following years as a legacy effect (Sang et al., 2019; Miller et al., 2023). Tree ring analysis in combination with historical climate data is therefore useful to determine limiting climate factors, such as moisture deficits. In combination with projected climate change, this information can inform forecasts of forest growth and carbon sequestration potential of forest ecosystems under climate change.

Tree ring analysis usually relies on evaluating annual radial increment from a wood core, taken at 1.3 m stem height. However, this approach does not necessarily provide the best estimate of growth and carbon sequestration potential through secondary growth along the

* Corresponding author at: Department of Silviculture and Forest Ecology of the Temperate Zones, Georg-August-University Göttingen, Büsgenweg 1, 37077 Göttingen, Germany.
E-mail address: lars.sprengel@uni-goettingen.de (L. Sprengel).

https://doi.org/10.1016/j.foreco.2023.121299
Received 25 April 2023; Received in revised form 16 July 2023; Accepted 22 July 2023
Available online 27 July 2023

whole stem. Somenguem Donfack et al. (2023) found for *Fagus sylvatica* L. that in managed stands diameter increment was greater at breast height compared to at crown base height, while the opposite was the case in unmanaged stands. Sprengel et al. (2018) compared dendrometer data from different pruning treatments at two different stem heights of *Acer pseudoplatanus* L. and *Prunus avium* L. and found an earlier growth onset for both tree species at the higher dendrometer location. Also, a higher annual radial increment could be observed at the higher dendrometer location in a selective pruning treatment for *P. avium*. On the other hand, Van der Maaten-Theunissen and Bouriaud (2012) found for *Abies alba* Mill. and *Picea abies* (L.) Karst. that basal area increment at three different stem heights are highly correlated. Nevertheless, correlations of annual radial increment at different stem heights are species-specific, and increments at multiple heights should be examined for reliable representation from increments at 1.3 m stem height.

Carbon sequestration of natural and planted forests in China is potentially of global relevance. China has the largest afforestation and reforestation programs in the world, with over 50 million hectares of farmlands and grasslands restored to forests over the last four decades, driven by the objective to raise forest cover from 5 to 15 % in northern China (Liu, 2014; Xu et al., 2019). China is also the largest emitter of CO_2 by country due to its population size, and is nevertheless aiming to be carbon neutral by 2060 (Mallapaty, 2020). To reach this ambitious goal, species-specific projections of climatic factors that limit forest growth and carbon sequestration potential plays a crucial role. In order to realize the long-term benefits for carbon sequestration through trees, natural and planted forests must remain healthy and productive over many decades. Therefore, afforestation and reforestation efforts need to focus on species selections and on regions that will support healthy and productive forests in the medium- and long-term under projected climate change.

Here, we contribute to the required knowledge base by investigating the climatic limiting factors for growth and carbon sequestration of eight economically important forest tree species in the Zhongtiao Mountain forestry region of Shanxi Province. This region is situated on the Loess Plateau of northeast China, where temperature and potentially also water deficits are expected to increase significantly by the end of the 21st century (She and Xia, 2018; Sun et al., 2019). Our specific objectives are to (1) quantify seasonal climatic limiting factors of tree growth for eight forest tree species, testing the working hypothesis that growth of some or all species may be seasonally restricted by moisture limitations; (2) derive a regionally relevant heat:moisture index that can be used as a predictor variable to forecast tree growth and carbon sequestration potential, and (3) use annual radial increments and wood density values to develop an annual carbon index to predict relative changes of carbon sequestration under future climate change scenarios.

2. Material and methods

2.1. Study area

The research area is located at the Zhongtiao Mountains in the southern Shanxi province of China (Fig. 1). According to the updated climate classification from Kottek et al. (2006), which is based on the Köppen (1918) system, the climate is classified as Monsoon-influenced hot-summer humid continental climate (Dwa). The region is subject to the East Asian Summer Monsoon, characterized by distinct hot and semi-humid summers and cold and dry winters (Li et al., 2013).

The area is dominated by coniferous forests, with *Pinus tabuliformis* Carrière as dominant tree species. For this study, we included three commercially important conifers: *P. tabuliformis*, *Pinus armandii* Franch. and *Larix principis-rupprechtii* Mayr, as well as five broadleaved tree species: *Quercus liaotungensis* Koidz., *Quercus variabilis* Blume, *Quercus aliena* Blume, *Quercus baronii* Skan and *Betula platyphylla* Sukaczev. Tree species names are according to the Tropicos data base (Missouri Botanical Garden, 2022).

2.2. Tree ring data

Trees were sampled representing a range of elevations found in the study area, from 750 m to about 1950 m. Trees selected for the collection

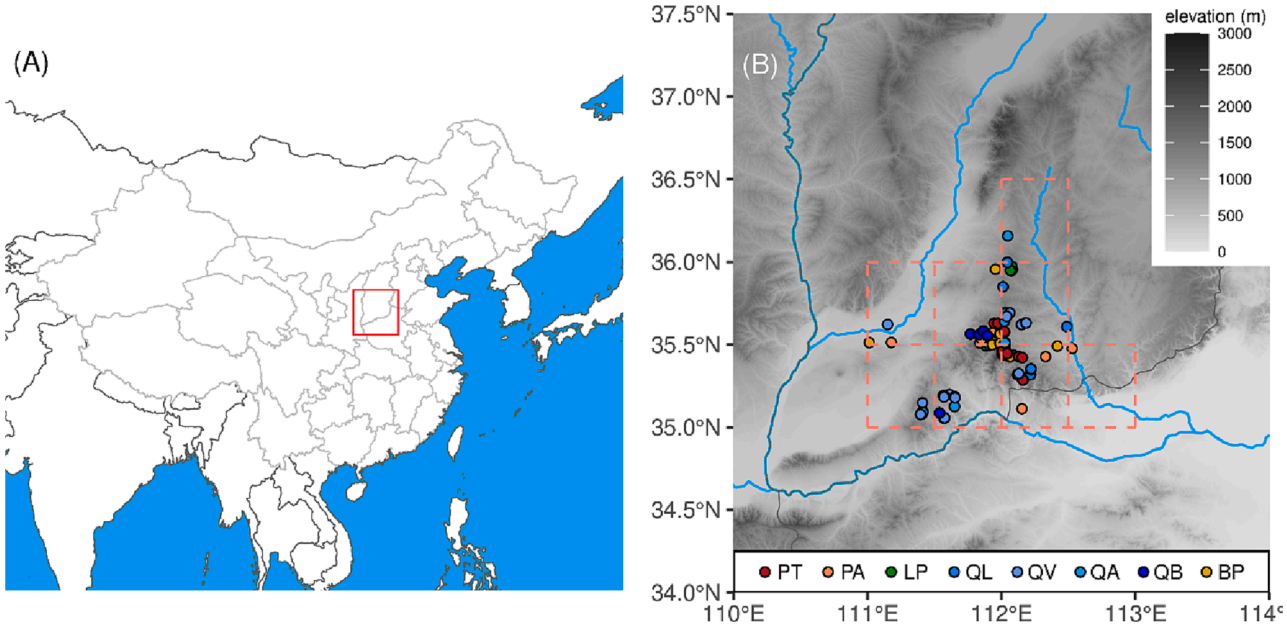

Fig. 1. (A) Map of China and surrounding eastern Asia. The red rectangle indicates the study area in southern Shanxi province; (B) Elevation map of southern Shanxi province (provincial boarders as black lines) showing the location of each sampled tree. Tree species are coded as PT for P. tabuliformis, PA for P. armandii, LP for L. principis-rupprechtii, QL for Q. liaotungensis, QV for Q. variabilis, QA for Q. aliena, QB for Q. baronii and BP for B. platyphylla. Red dashed rectangles depict grid cells for which historical climate variables were used. The maps were produced with Natural Earth data and Amazon Web Services Terrain Tiles using the packages rnaturalearth (South, 2017), elevatr (Hollister et al., 2021), furrr (Vaughan and Dancho, 2022), raster (Hijmans, 2021) and sf (Pebesma, 2018). (For interpretation of the references to color in this figure legend, the reader is referred to the web version of this article.)

of cross sections were taken exclusively from the predominant and dominant canopy layer, following recommendations by Kraft (1884). Samples were taken from monospecific stands that were not affected by gaps, skid trails or forest roads. Additionally, sample trees had healthy and evenly shaped crowns and no visible injuries, damages or infections, so that variability in growth over time was most likely caused by interannual variability in climate. Sample trees were felled and cross sections were sampled at 1.3 m, 3 m and 5 m stem heights. Sampling took place during the growing season of 2018. Additional information on selected trees by tree species is presented in Table 1.

Cross sections were air dried and sanded with a belt sander. Measurements of annual radial increment (ARI) were carried out with the software WinDENRO^{TM} (Régent Instruments Inc. 2012), where images of stem discs were digitally measured after obtaining high-resolution scans using a flatbed scanner (Microtek G10000). To obtain cross sectional averages of ARI arithmetic means from multiple radii – 8 at 1.3 m stem height and 4 at 3 m and 5 m stem height, respectively – were calculated. Crossdating for each tree species was carried out using the corr.rwl.seg function in the dplR package (Bunn, 2010). Each cross sectional average of ARI was detrended (I_{ARI}) using a smoothing spline utilizing the detrend function in dplR (Bunn et al., 2021). For subsequent climatic response function analyses, a relatively flexible smoothing spline was used with a flexibility parameter expressed in the number of years set to 15 years (nyrs = 15) whereas for calculating annual correlations and linear models with the heat:moisture index (H:MI) a relatively stiff smoothing spline was used staying at default of 67 % of each series length while in both cases the frequency response f was left at the default value of 0.5. After detrending for each tree species and each stem height a chronology of I_{ARI} was calculated using the chron function in dplR.

2.3. Wood density variations

To measure wood density variations high-frequency (HF) densitometry was applied (Schinker et al., 2003). Here, relative density variations along a straight line on the surface of a sample was measured utilizing the dielectric properties of the wood measured with a dielectric probe of 175 µm integration width (Torgovnikov, 1993). For each tree species a subsample of 5 cross sections at 1.3 m stem height were cut into 4 bars corresponding to the radii of the cardinal points and prepared for HF measurement using a diamond fly-cutter with air bearings to produce smooth surfaces (Spiecker et al., 2000). The relative density measured in volt is directly related to the ratio of cell wall to air filled lumen and is converted to air-dry volumetric mass density with approximately 12 % moisture content (ρ_{12}) using daily updated calibration functions (Wassenberg et al., 2014). These linear calibration functions are obtained using samples of known ρ_{12} from tropical diffuse porous tree species with little density variations (average $R^2 > 0.98$). Tree wise annual variations of ρ_{12} were also detrended towards index values (I ρ_{12}) in the same approach as ARI with the detrend function in dplR setting nyrs to 30 and the frequency response to 0.5.

2.4. Climate data

We used gridded monthly and annual air temperature averages and precipitation sums from Matsuura and Willmott (2018a, 2018b) for the historical time period 1900–2017. The data is provided on a 0.5 degree by 0.5 degree latitude/longitude grid with grid nodes being centered at the 0.25 degree. Monthly and annual averages were calculated based on all grid cells, where sample trees were located in (Fig. 1B).

For the annual correlation analyses, a heat:moisture index (H:MI) was calculated by dividing average air temperature in °C by precipitation sum in m, following Chen et al. (2010) and Rehfeldt et al. (1999). This index increases with increasing air temperature and decreasing precipitation and has the advantage that it can be calculated for different months of temperature and precipitation. In general, this approach can identify direct climate effects as well as legacy effects of precipitation in prior months through water stored in soils. We also tested for legacy effects of monthly climate from the prior growing season, through storage of photosyntates, but no significant effects were found (data not shown). Here, we used the average monthly air temperature of the current growing season for the months May-June and the precipitation sum of the months March-July. This monthly selection was informed by the response function analyses of multiple candidate H:MIs over different consecutive monthly periods for temperature and precipitation. The final H:MI metric for further analysis was selected based on the strength of the correlation between all tree species and each candidate H:MI.

For future predictions of the carbon index (I_C) for the climate normal 2041–2070, future monthly mean air temperature and precipitation sums from ClimateAP_v3.00 (Wang et al., 2017) were used to calculate H:MI. To cover the same area as for the historical climate data, we obtained future climate data for 32 evenly distributed locations within each grid cell, as the future climate data is provided in a 4 × 4 km downscaled resolution. The future climate data is based on an ensemble of 8 General Circulation Models (GCM) of the most recent iteration of the Coupled Model Intercomparison Project phase 6 (CMIP6) (Eyring et al., 2016) proposed by Mahony et al. (2022) using the emission scenario SSP2-4.5 (see Fig. 2 for a climate chart of this data). Future climate projections were added to the historical climate data that we used for tree ring analysis from Matsuura and Willmott (2018a, 2018b). Matching of the two data sets was carried out with the delta-method for a common 30-year climate normal period that is used as reference value. This reference period is typically chosen for a 30-year average where temporal and spatial weather station coverage is best and/or prior to a significant warming signal. In our case we chose the 1961–1990 period. All other layers (i.e. annual historical data and future projections) are then expressed and interpolated as anomaly (delta) from this long term climate mean. The approach has the advantage to be robust against missing values in weather station records for earlier periods, and it provides an effective bias correction of coarse scale projections to future climate.

Table 1
Tree species specific information of sample trees and of sampled stem heights.

tree species	sampled trees (n)	elevation (m a.s.L.)	tree rings (n)					
			1.3 m		3 m		5 m	
			mean	sd	mean	sd	mean	sd
P. tabuliformis	28	1187–1677	61	15	55	13	48	13
P. armandii	27	1338–1897	48	12	43	12	38	12
L. principis-rupprechtii	27	1191–1916	29	7	26	7	24	7
Q. liaotungensis	27	1283–1956	65	30	58	29	51	28
Q. variabilis	27	750–1223	51	13	49	14	44	13
Q. aliena	27	932–1350	57	15	50	14	44	13
Q. baronii	30	822–1459	46	18	38	19	25	15
B. platyphylla	27	1519–1927	38	18	36	17	31	15

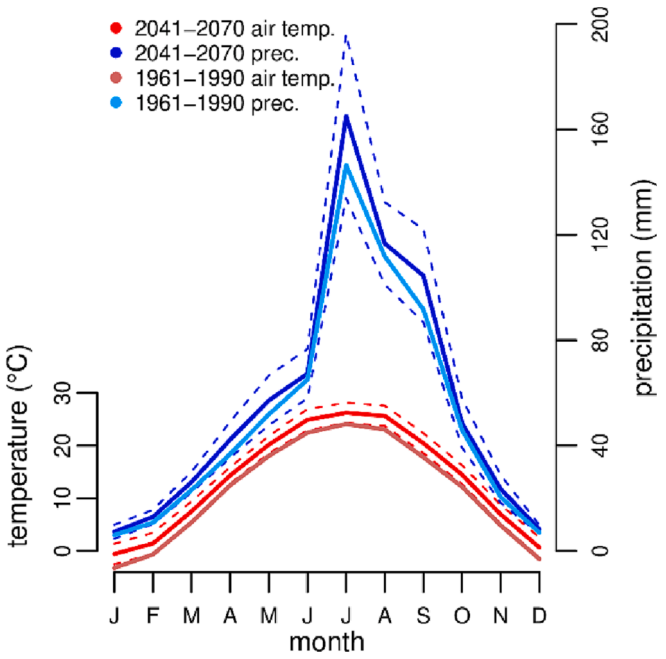

Fig. 2. Climate chart of the study area. The red and blue solid lines are showing monthly average air temperature and precipitation sums in the period 2041–2070, respectively, both averaged over the whole study region and with standard deviations as dashed lines. The light blue and light brown solid lines are showing the monthly average air temperature and precipitation sums in the period 1961–1990, respectively. (For interpretation of the references to color in this figure legend, the reader is referred to the web version of this article.)

2.5. Statistical analysis

To identify relationships between monthly climate and I_{ARI} we applied static bootstrapped response function analyses (Guiot, 1991) using the function dcc in the package treeclim (Zang and Biondi, 2015), where principal components of climate data are calculated and are related to I_{ARI} at 1.3 m stem height by multiple regression. Stationary bootstrapping (1000 iterations) was applied to obtain significance levels and confidence intervals. The analyses were carried out for each tree species using the monthly air temperature averages and precipitation sums averaged over all grid cells of the months January-October, although shorter periods were subsequently used in the derived H:MI.

For the assessment of annual climate on tree growth and carbon sequestration for each tree species Spearman's ρ as non-parametric correlation coefficient was calculated between H:MI and ARI, I_{ARI} and ρ_{12} at 1.3 m stem height, respectively, using the cor.test function. Additionally, I_C was calculated, where for each tree species I_{ARI} at 1.3 m stem height was multiplied by I ρ_{12}. This carbon index is a simple function of I_{ARI} as a proxy for annual variations in tree growth and I ρ_{12} to estimate annual variations in woody biomass growth. It is assumed that a content of 50 % of the woody biomass is carbon (Lamlom and Savidge, 2003), thus I_C can be used as a proxy for true variations in annually sequestered carbon. This I_C was also correlated with H:MI using the cor.test function.

To predict I_C for the future climate normal period 2041–2070, for each tree species a model using generalized least squares with a first-order temporal autocorrelative structure (AR(1)) was calculated using the gls function in the package nlme (Pinheiro et al., 2022):

$$y_i = \beta_0 + \beta_1 x_i + \varepsilon, \varepsilon_t = \phi\varepsilon_{t-1}$$

where y_i is the i th value of variable I_C at predictor variable x_i as H:MI and ε is the residual error term including the AR(1) model ε_t at observation time t with correlation parameter ϕ and the previous observation at t-1. Based on the generalized least squares I_C was predicted for future H:MI for the 2041–2070 climate period using the predictSE.glm function from the package AICcmodavg (Mazerolle, 2023), where standard errors of predictions are approximated based on the delta method.

All statistical analyses, calculations and graphical outputs were produced in R (R Core Team, 2021).

3. Results

3.1. Climatic limitations

Dentrended annual radial increment (I_{ARI}) of most tree species is significantly positively related to precipitation in June of the current growing season (Fig. 3). This is true for *P. tabuliformis*, *P. armandii*, *Q. variabilis*, *Q. aliena* and *Q. baronii*. Additionally, *P. tabuliformis*, *P. armandii*, *Q. liaotungensis* and *Q. aliena* relate also significantly positive to precipitation in May and only *P. armandii* in addition is significantly positively related to precipitation in July. Nevertheless, a clear common trend in all tree species but *B. platyphylla* can be seen, where for all or at least some summer months precipitation is positively influencing radial growth, even though not necessarily significantly at an α-level of 0.05.

A corresponding temperature effect is also apparent: Significant inverse relationships for air temperature in June were observed for *P. tabuliformis*, *P. armandii*, *Q. liaotungensis* and *Q. aliena* (Fig. 3). Additionally, *P. tabuliformis*, *Q. liaotungensis* and *Q. aliena* relate also significantly negatively to air temperature in May and *Q. aliena* is additionally significantly negatively related to air temperature in July. Also, for air temperature a clear common trend, even though not always significant at an α-level of 0.05, in all tree species was observed, where for all or at least some summer months temperature is limiting radial growth.

Based on the identified months, where precipitation and air temperature relate to and limit radial growth, multiple candidate heat: moisture indices (H:MIs) were derived and tested whether they correlate with I_{ARI} of each tree species. Candidate H:MIs based on mean air temperature for May-June and May-July as well as precipitation sums for March-June, March-July, February-June and February-July, respectively, were inspected for their Spearman's correlation coefficient ρ. The selected H:MI for further analyses based on its best correlation averaged over all tree species is derived from mean air temperature in May-June and precipitation sum in March-July (Table 2).

3.2. Stem-level biomass and carbon estimation

Detrended I_{ARI} of all 8 tree species at 1.3 m, 3 m and 5 m stem heights were compared within each species by superimposition (Fig. 4). It is evident that within all tree species interannual patterns are similar at different stem heights. Only at earlier years, where sample size is decreasing towards fewer trees, deviations from common synchronicity can be observed.

Also, H:MI and I_{ARI} at all stem heights are highly synchronous (Fig. 4). Especially in years of less annual radial increment, H:MI is greater than the average of 78.47, demonstrating the suitability of the derived H:MI for further climate analyses. Pronounced warm and dry summers can be observed in the years 1900, 1920, 1929, 1941, 1955, 1986 and 1997.

With regards to biomass and carbon sequestration potential, the results further show pronounced differences in average air-dry volumetric mass density of stems with approximately 12 % moisture content (ρ_{12}) between different tree species (Fig. 5). Of all investigated tree species, the ones with highest average ρ_{12} are *Q. baronii* (0.931 g cm^{-3}), *Q. aliena* (0.927 g cm^{-3}) and *Q. variabilis* (0.872 g cm^{-3}), tree species with intermediate ρ_{12} are *Q. liaotungensis* (0.754 g cm^{-3}) and *L. principis-rupprechtii* (0.652 g cm^{-3}) and with in average least ρ_{12} are *B. platyphylla* (0.577 g cm^{-3}), *P. tabuliformis* (0.557 g cm^{-3}) and *P. armandii* (0.462 g cm^{-3}).

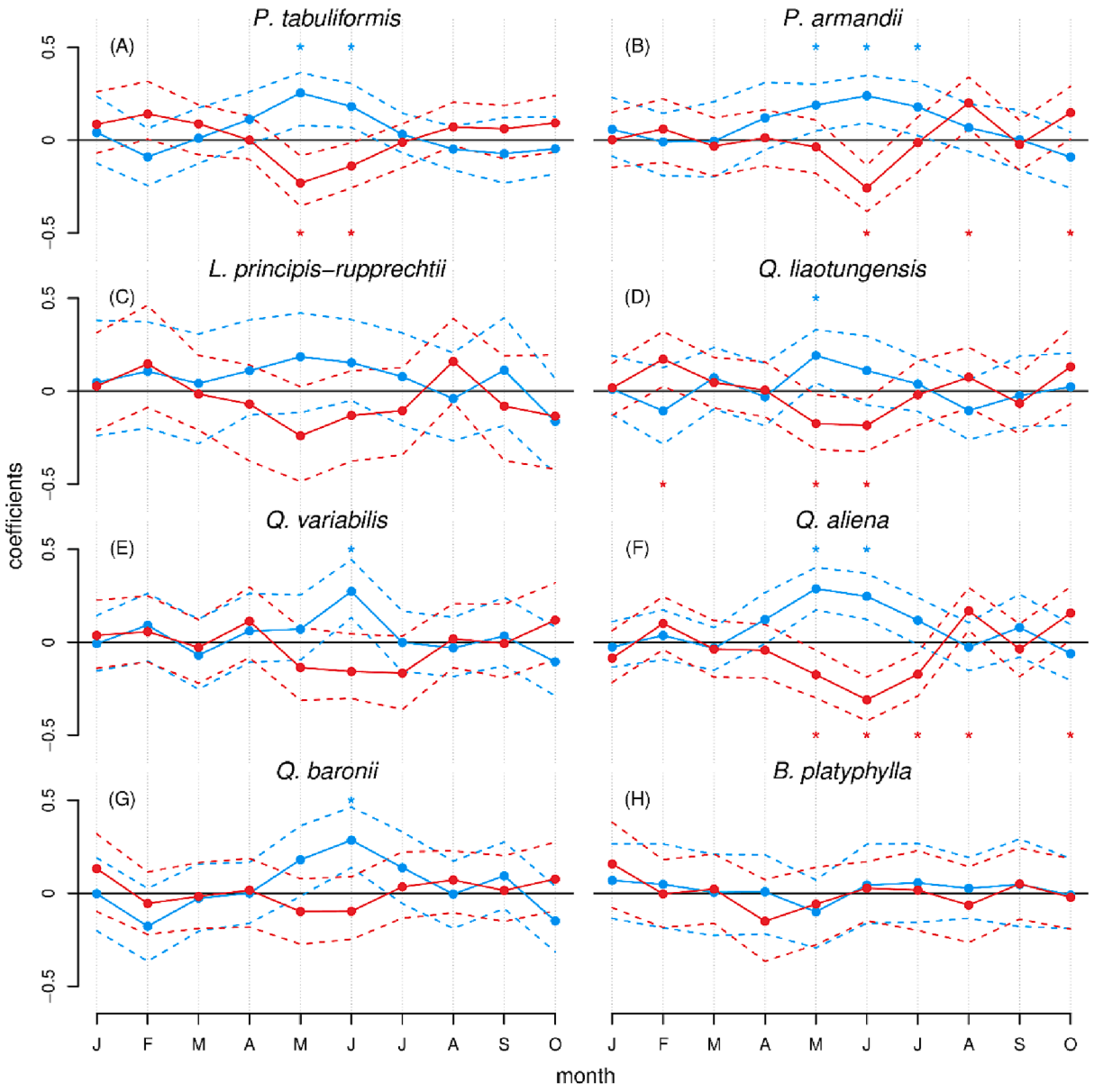

Fig. 3. Species wise coefficients of response function analyses at 1.3 m stem height for the months January-October of the current growing season. Blue solid lines and points represent coefficients related to monthly precipitation sums, red solid lines and points represent coefficients related to monthly air temperature averages. Dashed lines indicate the bootstrapped 95 % confidence intervals. Asteriscs in the corresponding color indicate significant results also based on bootstrapping. (For interpretation of the references to color in this figure legend, the reader is referred to the web version of this article.)

Table 2
Spearman's correlation coefficient ρ between indices of annual radial increment (I_{ARI}) at 1.3 m stem height for each tree species derived using a relatively stiff spline and best candidate heat moisture indices (H:MI) for different monthly time periods expressed as simplified formulas. Strongest average negative correlation indicated in bold.

tree species	$\frac{T_{MJ}}{P_{MAMJ}}$	$\frac{T_{MJ}}{P_{MAMJJ}}$	$\frac{T_{MJ}}{P_{FMAMJ}}$	$\frac{T_{MJ}}{P_{FMAMJJ}}$	$\frac{T_{MJJ}}{P_{MAMJ}}$	$\frac{T_{MJJ}}{P_{MAMJJ}}$	$\frac{T_{MJJ}}{P_{FMAMJ}}$	$\frac{T_{MJJ}}{P_{FMAMJJ}}$
P. tabuliformis	−0.421	−0.403	−0.421	−0.403	−0.422	−0.393	−0.422	−0.393
P. armandii	−0.376	−0.452	−0.378	−0.454	−0.381	−0.449	−0.383	−0.451
L. principis-rupprechtii	−0.52	−0.438	−0.535	−0.445	−0.517	−0.423	−0.533	−0.43
Q. liaotungensis	−0.223	−0.292	−0.18	−0.264	−0.217	−0.276	−0.173	−0.249
Q. variabilis	−0.299	−0.316	−0.295	−0.322	−0.304	−0.31	−0.3	−0.316
Q. aliena	−0.544	−0.59	−0.546	−0.596	−0.549	−0.58	−0.551	−0.587
Q. baronii	−0.293	−0.212	−0.272	−0.196	−0.295	−0.208	−0.274	−0.192
B. platyphylla	−0.059	−0.126	−0.062	−0.129	−0.059	−0.119	−0.062	−0.122
average	−0.342	**−0.354**	−0.336	−0.351	−0.343	−0.345	−0.337	−0.342

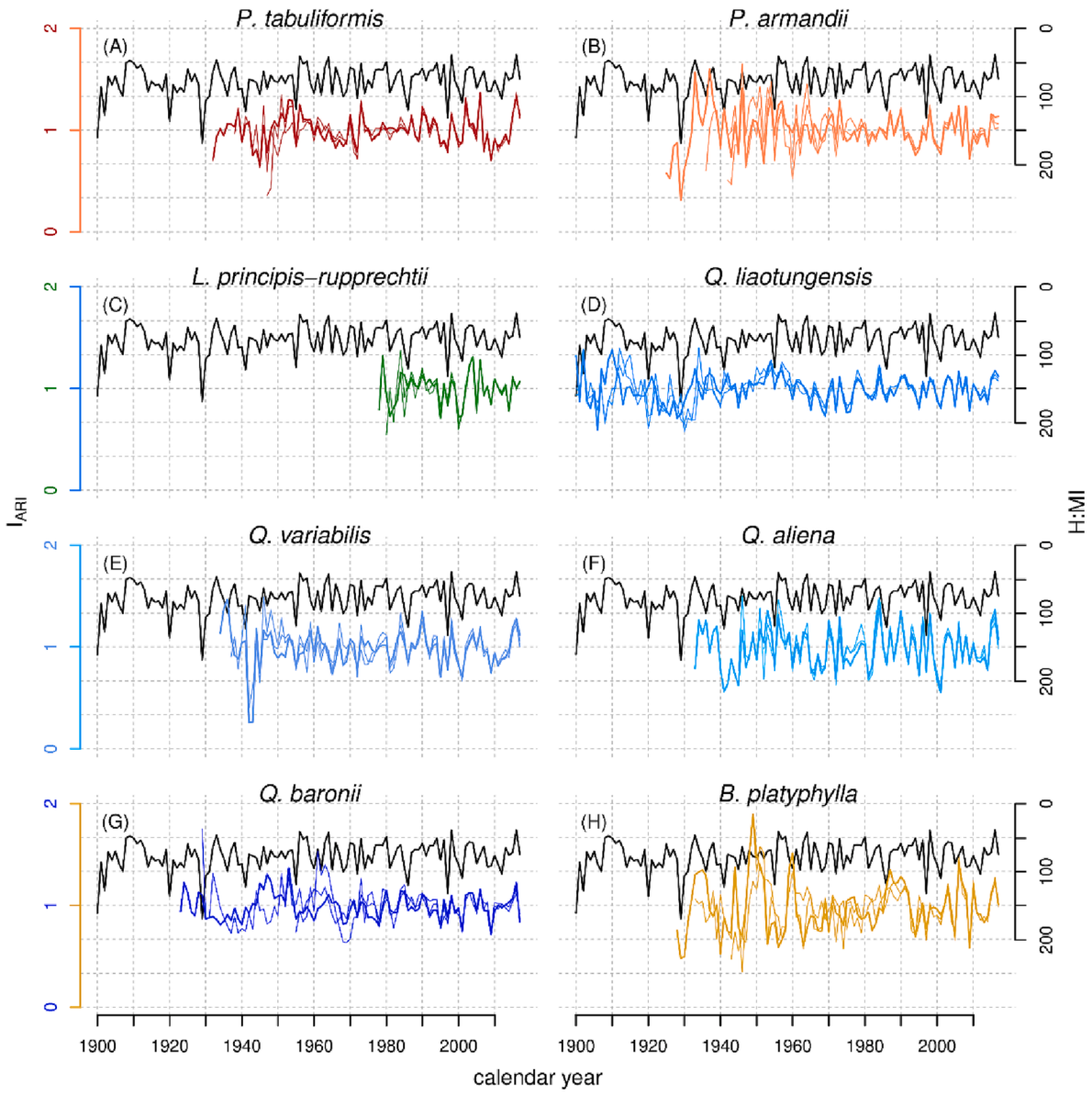

Fig. 4. Species wise indices of annual radial increment (I_{ARI}) derived using a relatively stiff smoothing spline; the bold colored curves represent I_{ARI} at 1.3 m stem height, the thin colored curves represent I_{ARI} at 3 and 5 m stem height, respectively. Black curves in each plot depict the same heat moisture index (H:MI).

Species wise annual synchronicity between detrended ρ_{12} (I ρ_{12}) and H:MI is not as evident as between H:MI and I_{ARI} (cf. Figs. 4 and 5). This can also be seen from Spearman's ρ, were correlation coefficients between H:MI and ARI and I_{ARI}, respectively, are highly negative for all investigated tree species but *B. platyphylla*, and close to 0 between H:MI and ρ_{12} (Fig. 6). However, species wise carbon indices (I_C) derived from I_{ARI} and I ρ_{12} shows also relatively high synchronicity and negative correlations for all investigated tree species but *B. platyphylla*, demonstrating the potential of H:MI as predictor to model I_C as a proxy for carbon sequestration.

3.3. Predicting future I_C

Based on the latest CMIP6 multimodel projections, water stress is not expected to increase for the study area. The H:MI estimate relevant for tree growth is predicted to decrease from 78.47 ± 23.04 in the used historical time period 1900–2017 to 65.9 ± 18.96 for the 2041–2070 future period. Species-wise generalized least squares with dependent variable I_C and predictor H:MI show highly significant negative relationships for *P. tabuliformis*, *P. armandii*, *L. principis-rupprechtii*, *Q. liaotungensis*, *Q. variabilis*, *Q. aliena* and *Q. baronii*. Therefore, I_C for these 7 tree species is predicted to increase in the climate normal period 2041–2070. For *B. platyphylla* no significant relationship was observed and no increase or decrease of H:MI in the climate normal period 2041–2070 is expected (Table 3).

4. Discussion

The results generally indicate that forest tree growth and carbon sequestration in the study region are trending near neutral or slightly positive. While we could find water limitations during the growing season that were consistent across all species, and statistically significant for all but one species, future climate change projections for the 2041–2070 period do not predict that water limitations will increase in the medium-term future. Based on species wise bootstrapped response function analyses we identified the climatic months in regard to precipitation sums and mean air temperature to which detrended annual radial increments (I_{ARI}) had the strongest responses. Coefficients show

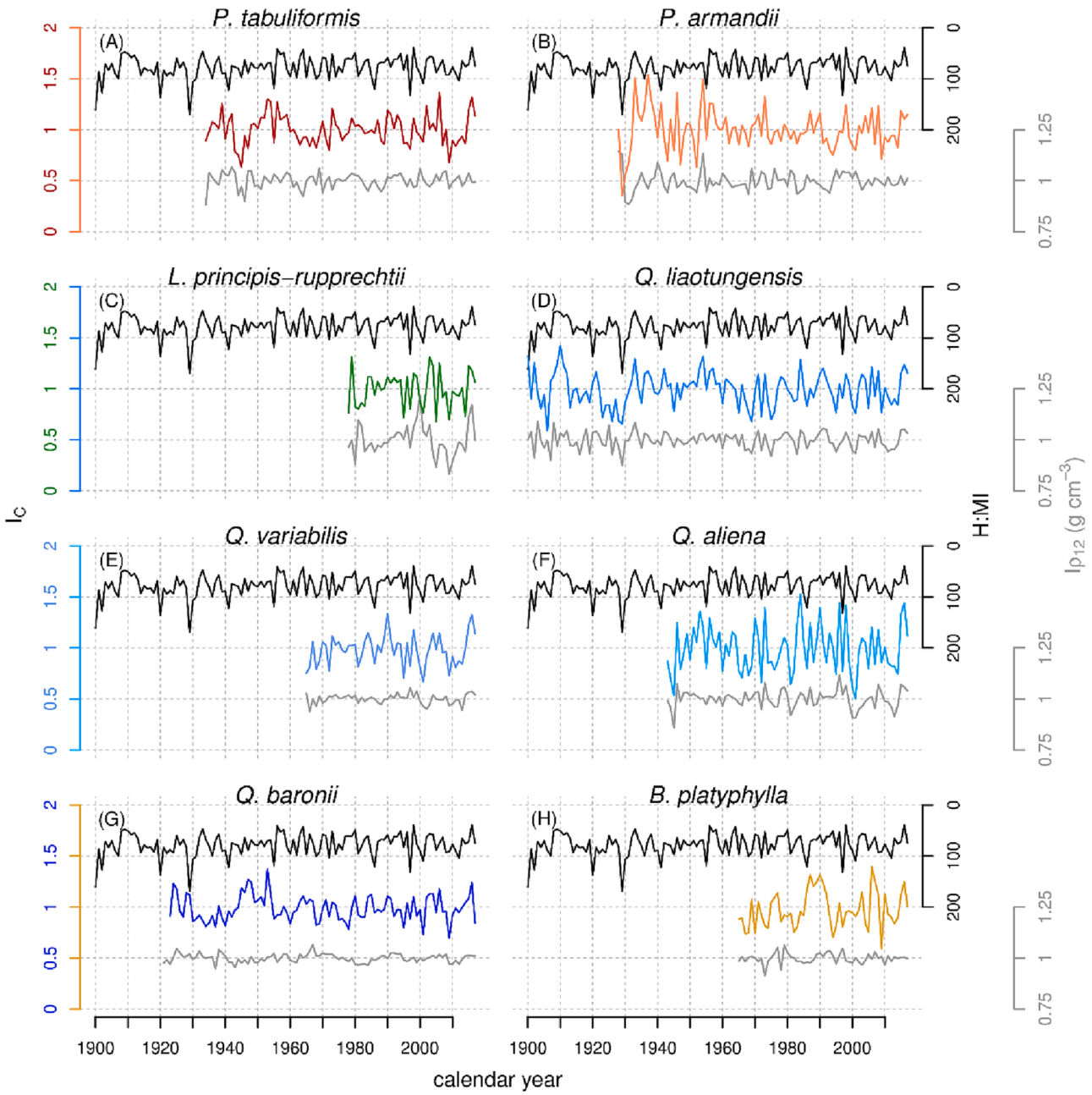

Fig. 5. Species wise annual variations of wood density index with 12 % moisture content (I ρ_{12}) at 1.3 m stem height are depicted as grey curves, annual values of carbon index (I_C) at 1.3 m stem height are shown as colored curves. Black curves in each plot depict the same heat moisture index (H:MI).

common patterns for all tree species but *B. platyphylla*: these are in general a positive response of radial increment to summer precipitation and a limitation from summer air temperature. Responses are more obvious for *P. tabuliformis*, *P. armandii* and *Q. aliena*, and less so for *L. principis-rupprechtii*, *Q. liaotungensis*, *Q. variabilis* and *Q. baronii*. In the case of *L. principis-rupprechtii* error bars are relatively wide so that coefficients are not significant. This is due to the short observation length for this tree species dating back only until 1978 (Fig. 4C). However, as the overall pattern is similar to that of the other conifer tree species it can be expected that an increase in observation length would turn coefficients of the summer months at least partly towards significance.

More in general, our results from the response function analyses are in line with results from Hipler et al. (2020), where for *P. tabuliformis* precipitation in June is positively related to I_{ARI} and air temperature in June is limiting. For *Larix gmelinii* (Rupr.) Kuzen., a species of which *L. principis-rupprechtii* was classified as variety in the past (Puhua and Lihuan, 1994), air temperature in May and June is significantly limiting I_{ARI}, substantiating our assumption that an increase in observation length would turn observed patterns in coefficients partly into significance. Furthermore, for *Quercus mongolica* Fisch. ex Ledeb., a close relative with whom *Q. liaotungensis* is hybridizing in areas of sympatry (Zeng et al., 2010), also June precipitation is promoting and June air temperature is limiting I_{ARI} significantly, as is observable for *Q. liaotungensis* in our analyses.

To ensure comparability between tree species for further analyses we formulated a single heat:moisture index (H:MI) identical to all tree species, even though in Table 2 different candidate H:MIs are correlating best with I_{ARI} of different tree species. Therefore, the in average best correlating H:MI was used for further analyses. The simple H:MI we selected here has the advantage that in general it can be calculated for different monthly periods of air temperature and precipitation sums (Hamann and Wang, 2005; Chen et al., 2010). This characteristic makes

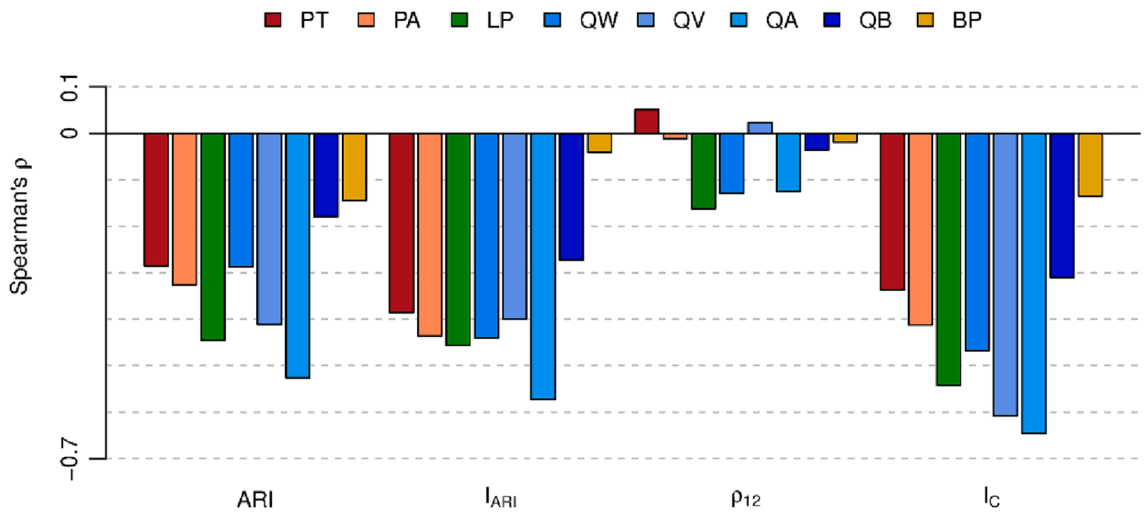

Fig. 6. Spearman's ρ between the same heat:moisture index (H:MI) and annual radial increment (ARI), indices of ARI derived using a relatively stiff smoothing spline (I_{ARI}), wood density variations with 12 % moisture content (ρ_{12}) and the carbon index (I_C), all at 1.3 m stem height, respectively. Tree species are coded as PT for *P. tabuliformis*, PA for *P. armandii*, LP for *L. principis-rupprechtii*, QL for *Q. liaotungensis*, QV for *Q. variabilis*, QA for *Q. aliena*, QB for *Q. baronii* and BP for *B. platyphylla*.

Table 3
Results of species wise linear models with the carbon index (I_C) as dependent variable and the heat moisture index (H:MI) as predictor. Estimates and standard errors of the carbon index for the historical period, and for the projected change in I_C for the climate normal period 2041–2070 as well as *p*-values for the slope are shown.

tree species	historical I_C	2041–2070 predicted I_C	*p*-value
P. tabuliformis	1.001 ± 0.146	1.026 ± 0.021	<0.001
P. armandii	0.999 ± 0.198	1.045 ± 0.025	<0.001
L. principis-rupprechtii	0.994 ± 0.173	1.032 ± 0.021	<0.001
Q. liaotungensis	0.994 ± 0.164	1.024 ± 0.02	<0.001
Q. variabilis	0.979 ± 0.148	1.021 ± 0.024	<0.001
Q. aliena	0.991 ± 0.234	1.063 ± 0.027	<0.001
Q. baronii	0.987 ± 0.125	1.004 ± 0.019	0.003
B. platyphylla	0.976 ± 0.181	0.991 ± 0.037	0.151

it superior for our approach compared to more common climate indices such as the Thornthwaite (1948) Index.

Fig. 4 well demonstrates the suitability of I_{ARI} at 1.3 m stem height to represent annual radial growth patterns of the entire stem for all 8 investigated tree species. However, this result does not indicate that average annual radial increment (ARI) is similar at different stem heights as detrended index values do not represent absolute values. Nevertheless, for the tree species in this study relative interannual changes at different stem heights can be retrieved from 1.3 m stem height.

To measure inter- and intra-annual wood density variation high-frequency densitometry is a common approach (Montwé et al., 2014; Wassenberg et al., 2015; Sprengel et al., 2020). Measured relative density based on dielectric properties is calibrated to volumetric mass density of air-dry wood with approximately 12 % moisture content (ρ_{12}). ρ_{12} itself may already be useful to serve as a proxy for biomass and carbon sequestration. However, the amount of carbon stored in the woody biomass depends also on the volume. Simple biomass indices have therefore been calculated by including for example basal area increment (BAI) as a simple proxy for volume (Soro et al., 2022). In our approach to calculate a carbon index (I_C) we include I_{ARI} instead of easy to calculate BAI, as BAI is increasing with age by a function to the power of 2, and detrended ρ_{12} (I ρ_{12}) as standardized annual variations of annual wood density. Our I_C based on I_{ARI} and I ρ_{12} therefore is stationary over time and can be used to identify annual relationships to H:MI, which are not masked by an age-trend.

Our species specific averages of ρ_{12} are matching well values from the literature, in general basic wood density (oven-dry mass divided by green volume, ρ_b), a more common value in the literature, more difficult to obtain and always less than ρ_{12}: Cheng (1985) gives for *P. tabuliformis* a ρ_b of 0.36 g cm^{-3} and for *Q. liaotungensis* 0.61 g cm^{-3}; Cheng (1992) states for *P. armandii* a ρ_b between 0.35 and 0.409 g cm^{-3}, for *L. gmelinii* between 0.528 and 0.599 g cm^{-3}, for *Q. variabilis* between 0.719 and 0.795 g cm^{-3}, for *Q. aliena* between 0.627 and 0.756 g cm^{-3} and for *B. platyphylla* between 0.489 and 0.546 g cm^{-3} (all values from the Global wood density database (Zanne et al., 2009). Our correlation analysis is showing that ρ_{12} is not systematically covarying with climatic variables for any tree species. This is typically more the case for the climate sensitive annual maximum latewood density of a variety of different tree species (e.g. Schweingruber et al., 1993; van der Maaten-Theunissen et al., 2012).

For the future climate variables monthly mean air temperature and precipitation sums we used an ensemble of 8 GCMs based on the most recent CMIP6 iteration. This ensemble is in line with IPCC's recent assessment of the very likely range of Earth's equilibrium climate sensitivity (Mahony et al., 2022). Also, 4 different emission scenarios following the major shared socioeconomic pathways marker scenarios are available: SSP1-2.6, SSP2-4.5, SSP3-7.0 and SSP5-8.5. We judged that SSP2-4.5, commonly called the "middle of the road" where trends do not shift noticeably compared to the past, was the most realistic scenario to select.

5. Conclusion

This study contributes evidence that forest tree growth and carbon sequestration of *P. tabuliformis*, *P. armandii*, *L. principis-rupprechtii*, *Q. liaotungensis*, *Q. variabilis*, *Q. aliena*, *Q. baronii* and *B. platyphylla* in Zhongtiao Mountains of Shanxi Province are trending near neutral or slightly positive. While we could find water limitations during the growing season that were consistent across all species, and statistically significant for all but one species, future climate change projections for the 2041–2070 period do not predict that water limitations will increase in the medium-term future, which should allow for productive forestry operations and carbon sequestration throughout the next generation of planted and naturally regenerated forests in the Zhongtiao Mountain forestry region of Shanxi Province, which will likely be representative of comparable ecological regions of north-eastern China. The results support the viability of continued afforestation and reforestation efforts in the study area, and are likely applicable to comparable forestry regions

of north-eastern China as well.

Author contributions

LS, SW and HS contributed to the study conception and design and performed the field work tasks. LS supervised and carried out the data acquisition with support from HS. LS and AH analyzed the data. All authors interpreted the results. LS led the writing of the manuscript and all authors commented and critically revised to draft versions.

Declaration of Competing Interest

The authors declare that they have no known competing financial interests or personal relationships that could have appeared to influence the work reported in this paper.

Data availability

Data will be made available on request.

Acknowledgments

The cross sections were collected, processed and scanned in collaboration with the staff from Zhongtiaoshan Forest Bureau and the Chinese Academy of Forestry, with special thanks to Yingjian Wu, Xinjian Zhang, Fujun Duan, Linlong Wang and Chao Zhang.

Funding

This work was supported by the German Federal Ministry of Education and Research [01LZ1701A]; the German Federal Ministry of Food and Agriculture [28I-010-01]; the special fund for basic scientific research of central level public welfare scientific research institutes [CAFYBB2020MC002].

Author contributions

LS, SW and HS contributed to the study conception and design and performed the field work tasks. LS supervised and carried out the data acquisition with support from HS. LS and AH analyzed the data. All authors interpreted the results. LS led the writing of the manuscript and all authors commented and critically revised to draft versions.

References

Babst, F., Bouriaud, O., Poulter, B., Trouet, V., Girardin, M.P., Frank, D.C., 2019. Twentieth century redistribution in climatic drivers of global tree growth. Sci. Adv. 5 (1).

Bonan, G.B., 2008. Forests and climate change: forcings, feedbacks, and the climate benefits of forests. Science 320 (5882), 1444–1449.

Bunn, A.G., 2010. Statistical and visual crossdating in R using the dplR library. Dendrochronologia 28 (4), 251–258. https://doi.org/10.1016/j.dendro.2009.12.001.

Bunn, Andy; Korpela, Mikko; Biondi, Franco; Campelo, Filipe; Mérian, Pierre; Qeadan, Fares; Zang, Christian (2021): dplR: Dendrochronology Program Library in R. Online verfügbar unter https://CRAN.R-project.org/package=dplR.

Chen, P.-Y., Welsh, C., Hamann, A., 2010. Geographic variation in growth response of Douglas-fir to interannual climate variability and projected climate change. Glob. Chang. Biol. 16 (12), 3374–3385. https://doi.org/10.1111/j.1365-2486.2010.02166.x.

Cheng, J., 1985. Wood Science. China Forestry Publishing, Beijing.

Cheng, J.C., 1992. Anatomy and Properties of Chinese Woods. Chinese Academy of Forestry, Beijing.

D'Orangeville, L., Houle, D., Duchesne, L., Phillips, R.P., Bergeron, Y., Kneeshaw, D., 2018. Beneficial effects of climate warming on boreal tree growth may be transitory. *communications* 9 (1), S. 3213. https://doi.org/10.1038/s41467-018-05705-4.

Eyring, V., Bony, S., Meehl, G.A., Senior, C.A., Stevens, B., Stouffer, R.J., Taylor, K.E., 2016. Overview of the Coupled Model Intercomparison Project Phase 6 (CMIP6) experimental design and organization. *Geosci. Model Dev.* 9 (5), 1937–1958. https://doi.org/10.5194/gmd-9-1937-2016.

Guiot, J., 1991. The bootstrapped response function analysis. Tree-Ring Bull. 51, 39–41.

Hamann, A., Wang, T.L., 2005. Models of climatic normals for genecology and climate change studies in British Columbia. Agric. For. Meteorol. 128 (3-4), 211–221.

Hijmans, Robert J. (2021): raster: Geographic Data Analysis and Modeling. Online verfügbar unter https://CRAN.R-project.org/package=raster.

Hipler, S.-M., Speicher, B., Sprengel, L., Kahle, H.-P., Spiecker, H., Wu, S., 2020. Impact of precipitation and temperature variability of the east Asian Summer Monsoon (EASM) on annual radial increment of selected tree species in Northeast China. *Forests* 11 (10), S. 1093. https://doi.org/10.3390/f11101093.

Hollister, Jeffrey; Shah, Tarak; Robitaille, Alec L.; Beck, Marcus W.; Johnson, Mike (2021): elevatr: Access Elevation Data from Various APIs. Online verfügbar unter https://github.com/jhollist/elevatr/.

IPCC (2021): Climate Change 2021: The Physical Science Basis. Contribution of Working Group I to the Sixth Assessment Report of the Intergovernmental Panel on Climate Change. Hg. v. V. Masson-Delmotte, Zhai P., A. Pirani, S. L. Connors, C. Péan, S. Berger, et al. Cambridge, UK, and New York, NY, USA.

Köppen, W. (1918): Klassifikation der Klimate nach Temperatur Niederschlag, und Jahreslauf. In: *Petermann's Mitteilungen* 64 (1), 193-203 and 243-248.

Kottek, M., Grieser, J., Beck, C., Rudolf, B., Rubel, F., 2006. World Map of the Köppen-Geiger climate classification updatedWorld Map of the Köppen-Geiger climate classification updated. metz 15 (3), 259–263.

Kraft, G., 1884. Beiträge zur Lehre von den Durchforstungen, Schlagstellungen und Lichtungshieben. Klindworth's Verlag, Hannover.

Lamlom, S.H., Savidge, R.A., 2003. A reassessment of carbon content in wood: variation within and between 41 North American species. Biomass Bioenergy 25 (4), 381–388. https://doi.org/10.1016/S0961-9534(03)00033-3.

Larysch, E., Stangler, D.F., Puhlmann, H., Rathgeber, C.B.K., Seifert, T., Kahle, H.-P., Rühr, N.K., 2022. The 2018 hot drought pushed conifer wood formation to the limit of its plasticity: Consequences for woody biomass production and tree ring structure. Plant Biol. J. 24 (7), 1171–1185.

Li, Q., Liu, Y.u., Song, H., Cai, Q., Yang, Y., 2013. Long-term variation of temperature over North China and its links with large-scale atmospheric circulation. Quart. Int. 283, 11–20. https://doi.org/10.1016/j.quaint.2012.03.017.

Liu, Jianguo (2014): Forest Sustainability in China and Implications for a Telecoupled World. In: *Asia & Pacific Policy Stud* 1 (1), S. 230–250. DOI: 10.1002/app5.17.

Mahony, C.R., Wang, T., Hamann, A., Cannon, A.J., 2022. A global climate model ensemble for downscaled monthly climate normals over North America. Intl. J. Climatol. 42 (11), 5871–5891.

Mallapaty, S., 2020. How China could be carbon neutral by mid-century. Nature 586 (7830), 482–484.

Matsuura, Kenji; Willmott, Cort J. (2018a): Terrestrial Air Temperature: 1900-2017 Gridded Monthly Time Series. Version 5.01. Department of Geography, University of Delaware. Online verfügbar unter http://climate.geog.udel.edu/~climate/html_pages/Global2017/README.GlobalTsT2017.html, zuletzt geprüft am 14.09.2022.

Matsuura, Kenji; Willmott, Cort J. (2018b): Terrestrial Precipitation: 1900-2017 Gridded Monthly Time Series. Version 5.01. Department of Geography, University of Delaware. Online verfügbar unter http://climate.geog.udel.edu/~climate/html_pages/Global2017/README.GlobalTsP2017.html, zuletzt geprüft am 14.09.2022.

Mazerolle, Marc J. (2023): AICcmodavg: Model selection and multimodel inference based on (Q)AIC(c). Online verfügbar unter https://cran.r-project.org/package=AICcmodavg.

Miller, T.W., Stangler, D.F., Larysch, E., Honer, H., Puhlmann, H., Schindler, D., Jung, C., Seifert, T., Rigling, A., Kahle, H.-P., 2023. Later growth onsets or reduced growth rates: What characterises legacy effects at the tree-ring level in conifers after the severe 2018 drought? Sci. Total Environ. 854, 158703.

Missouri Botanical Garden (2022): Tropicos. Online verfügbar unter https://.tropicos.org, zuletzt geprüft am 04.10.2022.

Montwé, D., Spiecker, H., Hamann, A., 2014. An experimentally controlled extreme drought in a Norway spruce forest reveals fast hydraulic response and subsequent recovery of growth rates. Trees 28 (3), 891–900. https://doi.org/10.1007/s00468-014-1002-5.

Pan, Y., Birdsey, R.A., Fang, J., Houghton, R., Kauppi, P.E., Kurz, W.A., Phillips, O.L., Shvidenko, A., Lewis, S.L., Canadell, J.G., Ciais, P., Jackson, R.B., Pacala, S.W., McGuire, A.D., Piao, S., Rautiainen, A., Sitch, S., Hayes, D., 2011. A large and persistent carbon sink in the world's forests. Science 333 (6045), 988–993.

Pebesma, E., 2018. Simple features for R: standardized support for spatial vector data. *R Journal* 10 (1), 439–446. https://doi.org/10.32614/RJ-2018-009.

Pinheiro, J.; Bates, D.; R Core Team (2022): nlme: Linear and Nonlinear Mixed Effects Models. R package version 3.1-160. Online verfügbar unter https://CRAN.R-project.org/package=nlme.

Puhua, H., Lihuan, Z., 1994. Larix gmelinii. In: Roloff, A., Weisgerber, H., Lang, U.M., Stimm, B. (Eds.), Enzyklopädie der Holzgewächse. Handbuch und Atlas der Dendrologie. Wiley VCH, Weinheim, pp. 1–6.

R Core Team, 2021. R: A Language and Environment for Statistical Computing. Vienna, Austria. Online verfügbar unter https://www.R-project.org/.

Régent Instruments Inc, 2012. WinDENDRO™ 2012 For Tree-Ring Analysis. Régent Instruments Inc, Quebec City, Canada.

Rehfeldt, Gerald E.; Ying, Cheng C.; Spittlehouse, David L.; Hamilton, David A. (1999): Genetic responses to climate in Pinus contorta: niche breadth, climate change, and reforestation. In: *Ecological Monographs* 69 (3), S. 375–407. DOI: 10.1890/0012-9615(1999)069[0375:GRTCIP]2.0.CO;2.

Sang, Z., Sebastian-Azcona, J., Hamann, A., Menzel, A., Hacke, U., 2019. Adaptive limitations of white spruce populations to drought imply vulnerability to climate change in its western range. *Evolut. Appl.* 12 (9), 1850–1860. https://doi.org/10.1111/eva.12845.

Schinker, M.G., Hansen, N., Spiecker, H., 2003. High-frequency densitometry-a new method for the rapid evaluation of wood density variations. *IAWA J.* 24 (3), 231–239.

Schweingruber, F.H., Briffa, K.R., Nogler, P., 1993. A tree-ring densitometric transect from Alaska to Labrador. Int. J. Biometeorol. 37 (3), 151–169.

She, D., Xia, J., 2018. Copulas-based drought characteristics analysis and risk assessment across the Loess Plateau of China. Water Resour Manage 32 (2), 547–564.

Somenguem Donfack, L., Schall, P., Mund, M., Knohl, A., Ammer, C., 2023. Effects of competition reduction on intra-annual radial growth of European beech (*Fagus sylvatica* L.) at stem base and crown base. Trees – Structure and Function 37, 435–447. https://doi.org/10.1007/s00468-022-02360-7.

Soro, André; Lenz, Patrick; Roussel, Jean-Romain; Larochelle, François; Bousquet, Jean; Achim, Alexis (2022): The phenotypic and genetic effects of drought-induced stress on apical growth, ring width, wood density and biomass in white spruce seedlings. In: *New Forests*. DOI: 10.1007/s11056-022-09939-5.

South, Andy (2017): rnaturalearth: World Map Data from Natural Earth. Online verfügbar unter https://CRAN.R-project.org/package=rnaturalearth.

Spiecker, H., Schinker, M.G., Hansen, J., Park, Y.-I., Ebding, T., Döll, W., 2000. Cell structure in tree rings: novel methods for preparation and image analysis of large cross sections. *IAWA J.* 21 (3), 361–373.

Sprengel, L., Stangler, D., Sheppard, J., Morhart, C., Spiecker, H., 2018. Comparative analysis of the effects of stem height and artificial pruning on seasonal radial growth dynamics of wild cherry (Prunus avium L.) and Sycamore (Acer pseudoplatanus L.) in a widely spaced system. *Forests* 9 (4), S. 174. https://doi.org/10.3390/f9040174.

Sprengel, L., Cheng, Z., Hipler, S.-M., Wu, S., Spiecker, H., 2020. Mean annual wood density variations of Larix gmelinii (Rupr.), Quercus mongolica Fisch. ex Ledeb., and Pinus tabulaeformis Carr. at Two Different Stem Heights. Forests 11 (4), 394.

Sun, C.X., Huang, G.H., Fan, Y., Zhou, X., Lu, C., Wang, X.Q., 2019. Drought occurring with hot extremes: changes under future climate change on Loess Plateau, China. *Earth's Future* 7 (6), 587–604. https://doi.org/10.1029/2018EF001103.

Thornthwaite, C.W., 1948. An approach toward a rational classification of climate. Geogr. Rev. 38 (1), 55–94.

Torgovnikov, G.I., 1993. Dielectric Properties of Wood and Wood-Based Materials. Springer, Berlin Heidelberg, Berlin, Heidelberg.

van der Maaten-Theunissen, M., Bouriaud, O., 2012. Climate–growth relationships at different stem heights in silver fir and Norway spruce. Can. J. For. Res. 42 (5), 958–969. https://doi.org/10.1139/x2012-046.

van der Maaten-Theunissen, Marieke; Boden, Simon; van der Maaten, Ernst (2012): Wood density variations of Norway spruce (Picea abies (L.) Karst.) under contrasting climate conditions in southwestern Germany. In: *Annals of Forest Research* 56 (1), S. 91–103.

Vaughan, Davis; Dancho, Matt (2022): furrr: Apply Mapping Functions in Parallel using Futures. Online verfügbar unter https://CRAN.R-project.org/package=furrr.

Walker, A.P., De Kauwe, M.G., Bastos, A., Belmecheri, S., Georgiou, K., Keeling, R.F., McMahon, S.M., Medlyn, B.E., Moore, D.J.P., Norby, R.J., Zaehle, S., Anderson-Teixeira, K.J., Battipaglia, G., Brienen, R.J.W., Cabugao, K.G., Cailleret, M., Campbell, E., Canadell, J.G., Ciais, P., Craig, M.E., Ellsworth, D.S., Farquhar, G.D., Fatichi, S., Fisher, J.B., Frank, D.C., Graven, H., Gu, L., Haverd, V., Heilman, K., Heimann, M., Hungate, B.A., Iversen, C.M., Joos, F., Jiang, M., Keenan, T.F., Knauer, J., Körner, C., Leshyk, V.O., Leuzinger, S., Liu, Y., MacBean, N., Malhi, Y., McVicar, T.R., Penuelas, J., Pongratz, J., Powell, A.S., Riutta, T., Sabot, M.E.B., Schleucher, J., Sitch, S., Smith, W.K., Sulman, B., Taylor, B., Terrer, C., Torn, M.S., Treseder, K.K., Trugman, A.T., Trumbore, S.E., van Mantgem, P.J., Voelker, S.L., Whelan, M.E., Zuidema, P.A., 2021. Integrating the evidence for a terrestrial carbon sink caused by increasing atmospheric CO2. New Phytol. 229 (5), 2413–2445.

Wang, T., Wang, G., Innes, J.L., Seely, B., Chen, B., 2017. ClimateAP: an application for dynamic local downscaling of historical and future climate data in Asia Pacific. *Front. Agr. Sci. Eng.* 4 (4), 448.

Wassenberg, M., Montwé, D., Kahle, H.-P., Spiecker, H., 2014. Exploring high frequency densitometry calibration functions for different tree species. Dendrochronologia 32 (3), 273–281. https://doi.org/10.1016/j.dendro.2014.07.001.

Wassenberg, M., Chiu, H.-S., Guo, W., Spiecker, H., 2015. Analysis of wood density profiles of tree stems: incorporating vertical variations to optimize wood sampling strategies for density and biomass estimations. Trees 29 (2), 551–561. https://doi.org/10.1007/s00468-014-1134-7.

Williams, A.P., Cook, E.R., Smerdon, J.E., Cook, B.I., Abatzoglou, J.T., Bolles, K., Baek, S. H., Badger, A.M., Livneh, B., 2020. Large contribution from anthropogenic warming to an emerging North American megadrought. Science 368 (6488), 314–318.

Xu, Z., Chau, S.N., Ruzzenenti, F., Connor, T., Li, Y., Tang, Y., Li, D., Gong, M., Liu, J., 2019. Evolution of multiple global virtual material flows. Sci. Total Environ. 658, 659–668.

Zang, C., Biondi, F., 2015. treeclim: an R package for the numerical calibration of proxy-climate relationships. Ecography 38 (4), 431–436. https://doi.org/10.1111/ecog.01335.

Zanne, Amy E.; Lopez-Gonzalez, G.; Coomes, David A.; Ilic, Jugo; Jansen, Steven; Lewis, Simon L. et al. (2009): Data from: Towards a worldwide wood economics spectrum.

Zeng, Y.-F., Liao, W.-J., Petit, R.J., Zhang, D.-Y., Ingvarsson, P.K., 2010. Exploring species limits in two closely related Chinese oaks. *PLoS One* 5 (11), e15529.